

# Measurement of Deformation and Strain in Flip Chip on BGA (FC-BGA)

L. Kehoe, V. Guénebaut, P.V. Kelly,  
Optical Metrology Innovations Ltd.

2200 Cork Airport Business Park, Cork Airport, Co. Cork, Ireland  
Corresponding Author: liam.kehoe@optical-metrology.com

## Abstract

An autofocus Digital Image Correlation (DIC) workstation incorporating image stacking functionality was used to perform a thermo-mechanical deformation and strain analysis of controlled collapse chip connect (C4) bumps in two FC-BGA packages. Cross-sections through C4 bumped region were analysed through a temperature cycle from ambient temperature up to 100°C. Strain concentrations at the C4 layer-to-die interface are revealed. Aspects of recent advances in digital image correlation technology are described in the context of this study.

## Flip-chip “C4” interconnect advantages and issues

Flip chip interconnection offers many advantages over more traditional packaging technologies such as surface mount and plastic quad flat pack. These advantages include the ability to address the higher chip I/O density and finer I/O pitch demanded by the wireless communications industry, as well as offering cheaper fabrication costs and an ability to package large die, in stacked packages if required. However, there are also disadvantages that affect flip chip technology. One of the big issues facing designers of flip chip on BGA (FC-BGA) technology at present relates to the thermo-mechanical strain at controlled collapse chip connect (C4) bumps and in the underfill layer around them.

The mismatch in the coefficient of thermal expansion (CTE) that exists between a silicon chip and a printed wiring board substrate contributes to thermally driven stress and can affect package reliability in many ways. Particular interest is focused on the behaviour of the C4 bumps and surrounding underfill material as a function of temperature. This layer is often the location of highly localised strain. In the particular case of larger die sizes, the provision of strain relief for the C4 bumps faces many technical challenges. As package designers use innovative designs and novel materials for their packages, next generation metrology tools are required to address CTE mismatch issues, to experimentally verify the performance of these designs and materials, and to complement Finite Element Analysis and older metrology techniques.

## Digital Image Correlation Deformation Measurement

An autofocus Digital Image Correlation (DIC) workstation incorporating image stacking functionality and a Successive Approximation Non-integral Pixel Shifting (SA-NPS) algorithm was used to perform deformation and strain analyses of the C4 bump interconnect region of FC-BGA packages. This type of advanced digital image correlation technology has been shown to be capable of measuring deformation on microtextured cross-sectioned electronic package materials to 0.05 pixel where multiple materials are visible in the field of view [1,2], and to 0.02 pixel where a

single material fills the field of view, in similar configurations to this work.

imaging the sample through a long working distance objective. A CCD camera records stacks of digital images as the sample surface is translated vertically through the focal plane of the objective.

Digital image correlation has a number of advantages of laser-based and interferometry. The technique uses incoherent colour-filtered white light, in non-interferometric technology, and is therefore less susceptible to mirage convection effects and dust than comparable laser-based interferometers. It does not require any special structure or pattern to be applied to the sample, nor does it require stereoscopic imaging.

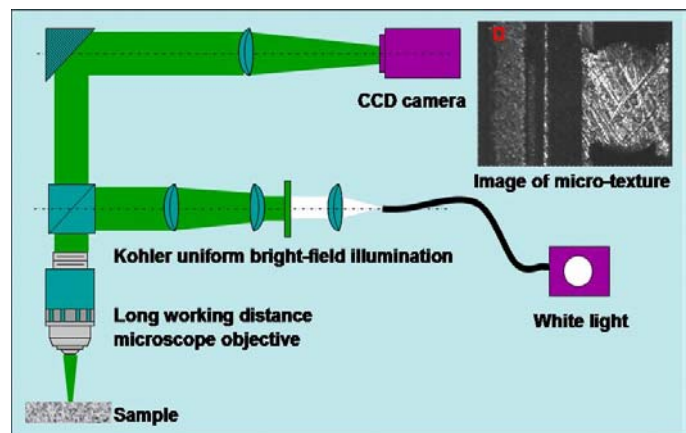


Figure 1. Digital Image Correlation Optical System

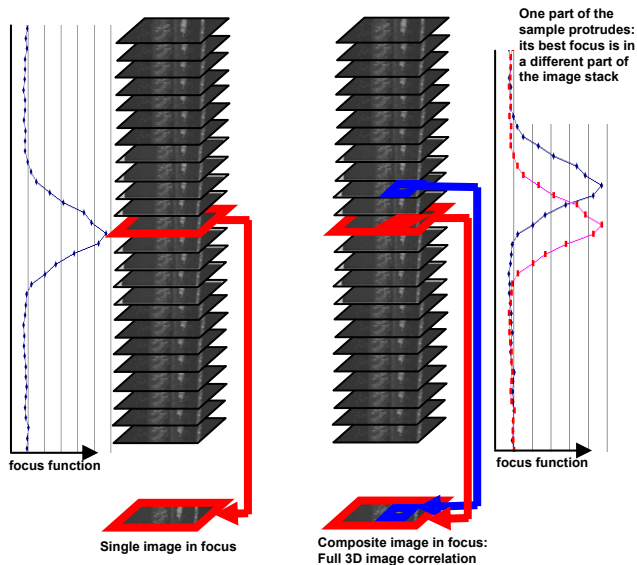
## Image stacking and autofocus

An operator-independent autofocus capability at every measurement temperature is key to the implementation of digital image correlation for thermo-mechanical deformation measurement. While Moiré technology [3,4] is only useful in the case of flat samples, and required a high precision grating structure to be applied, the advanced digital image correlation technology with image stacking and multi-area autofocusing may be used on samples which have a bumpy or tilted surface, and is capable of finding focus on a flat background even with a protruding solder bump in the field of view. This not only simplifies sample preparation but also increases the accuracy of DIC because of its sensitivity to accurate focus, especially at elevated temperatures. As this is an optical technique the correction of sample tilt or protrusions when focussing has dramatic effects on the accuracy of higher magnification and sensitivity measurements.

Image stacking is the key to obtaining an objective autofocus function. This advanced technology is more complex than the simple correlation of a pair of images, and instead uses a full 3-D image stack to achieve the best image in focus, at each measurement point in the thermal stress

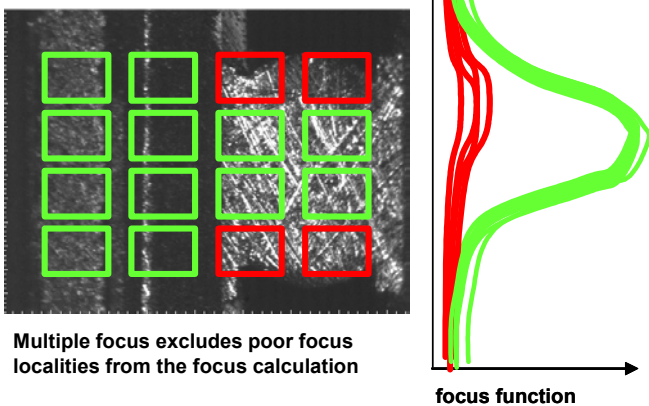
cycle. If required, parts of the image in focus can be composed of sub-images from more than one layer of the 3-D stack. This technology also allows the extraction of 3-D information using a single camera, and obviates the need for stereoscopic or multiple camera / off-axis imaging systems.

Figure 2 shows the manner in which a stack of images is made through the region of focus of the optical system, and the way in which the image in focus can be selected or composited. The Fast Fourier Transform focus function is the key to the autofocus process, and can be evaluated for many parts of an image. The concept of multiple area focusing (Figure 3) has been developed to allow focusing on a flat region having some curved protruding or recessed regions.



**Figure 2. Image stacking principle.** The 3D stack of images is acquired and processed by Fast Fourier Transform to auto-select single 2D best focus image (left) or in full 3D capability, to auto-select the best focus regions of different stack images and render them as composite image in focus.

Part of the sample is curved and has a poor local focus



**Figure 3. Multiple area focusing excludes regions of poor focus and focuses on the flat regions of the sample ignoring the protrusions and voids.**

The measurement accuracy increases when the correlation is done after rigid body motion correction, as shown in Figure 4. The rigid body translation vector is determined at each temperature from a single in-focus image correlated to the image at the previous temperature. The sample is physically translated back to within one pixel of its original reference position, before measurement of the full image stack.

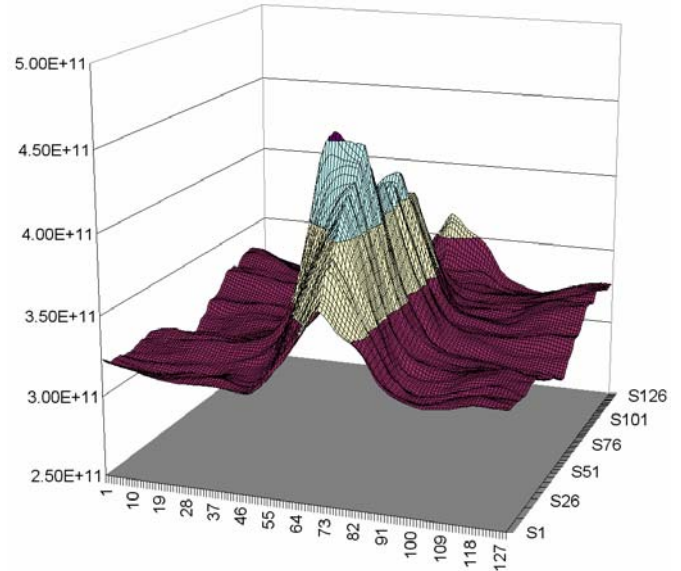


**Figure 4. Cross-correlation coefficient versus rigid body movement.** The vertical axis shows the correlation coefficient value for an image with a rigid body motion shown in the X and Y plane.

Digital Image Correlation is performed by dividing the 10-bit, 1.92 megapixel reference image into typically 1 kilopixel (32 X 32 pixel) blocks or subimages, which constitute a unique digital fingerprint of the local area of the sample under inspection. An example of a kilopixel subimage derived from the solder ball in Figure 4, is shown in Figure 5. Quarter-kilopixel subimages can also be used with reduced precision. The SA-NPS correlation algorithm calculates the displacement vector of each subimage in the reference image, to its location in the image recorded after the temperature change. It does this calculation to deep sub-pixel precision, by fractional pixel shifting of the digital greyscale pattern of each subimage, using a hill-climbing algorithm to find the subpixel x-y motion corresponding to the correlation coefficient peak.

The SA-NPS calculation is independently performed on every kilopixel image in the field of view. Moreover, by overlapping the subimage sampling, multiple displacement vectors may be calculated to full precision across the area of a single subimage.

The basic result of the calculation is shown in the form of a deformation map, composed of these vectors showing the in-plane displacement of each area of the sample. Particular characteristics of the sample can also be shown by deriving graphs from the raw data. These maps show the shear and strain present in the sample.

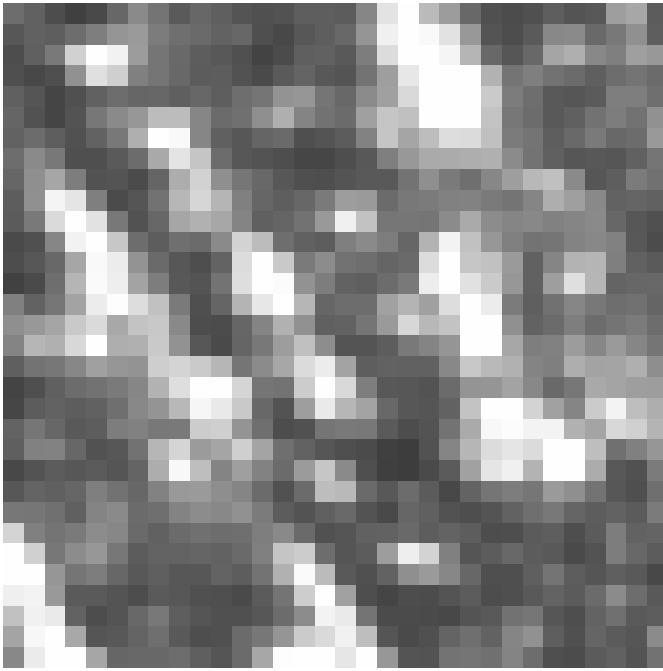


**Figure 5. A 32 X 32 pixel subimage (10-bit greyscale).** This subimage constitutes a digital fingerprint whose motion can be tracked to deep sub-pixel resolution.

### Deformation Map

The deformation map shows the sample deformation, in other words the displacement of each area of the sample between two temperatures. Deformation maps are typically corrected for rigid body motion, and the resultant of all the vectors within the reference area used for this correction is zero. A small local zero reference area can be user-defined at any local area in the field of view, and the vectors re-plotted.

The deformation map shows the resultant deformation of the x-deformation (u) and y-deformation (v) vectors, but can also be displayed as a contour map for either the u or v component alone.

The deformation map has two scales, one for the micrograph and a magnified scale for the vectors. The image scale is depicted on the captured video microscope images, and its resolution is limited by the optical system and camera characteristics, ultimately being limited by diffraction. The deformation vector scale is that of the deformation vectors superimposed on the reference image, and has a deep sub-pixel resolution. To display the measurable sub-micron deformation, overlay vectors are plotted on a scale of typically 5 to 50 times that of the image. Examples of deformation maps are shown in Figure 13, 14, 16 and 17.

### Shear Map

The shear map is related to the rotation of the sides a square defined by its four corners, the four corners being the origins of four deformation measurements.

The normal shear value is given by the equation:

$$\gamma = \frac{1}{2}(\theta_1 + \theta_2)$$

By using an approximation caused by the fact that the angles of deformation are infinitesimal, one can transform this to the following equation:

$$\gamma = \frac{1}{2} \left( \frac{\delta u}{\delta x} + \frac{\delta v}{\delta y} \right)$$

Shear maps are represented as contour maps, an example of which is shown in figure 15.

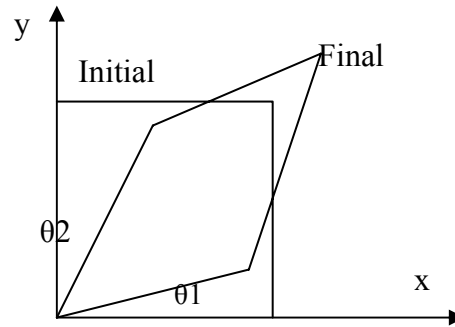


**Figure 6. Diagram showing the physical representation of a shear calculation.**

### Strain in X

The X strain map is a basic derivative of the deformation map along the X axis of the map, and can be displayed as a contour map. The function is the following:

$$\epsilon_x = \left( \frac{\delta u}{\delta x} \right)$$

### Strain in Y

A similar function can be computed for the Y axis.

$$\epsilon_y = \left( \frac{\delta v}{\delta y} \right)$$

### Combined Strain

The combined strain calculates the strain imposed on one point by all neighbouring points.

$$\epsilon = \left( \left( \sum_{i=1}^N \frac{\delta x}{x} \right)^2 + \left( \sum_{i=1}^N \frac{\delta y}{y} \right)^2 \right)^{\frac{1}{2}}$$

Because of the dropoff in the strain imposed on the point with respect to the distance between the point and the neighbour, and due to the square nature of our mesh, the equation can be simplified to include only the 8 nearest neighbours. It can be shown as a contour map for the magnitude, and as a vector map for the resultant direction of strain at each point.

### Resolution of DIC

The resolution of the DIC technique depends on a number of factors, but primarily on the magnification of the optics used. The vector origin pitch is a measure of the lateral resolution of the technique. The displacement resolution is a measure of the smallest resolvable change in the magnitude of a displacement vector.

Table 1 illustrates the achievable resolution obtainable.

Objective magnification	Field of view (mm)	Vector origin pitch*# (μm)	Displacement Resolution* (nm)
X 2	4.0 X 3.0	45	125
X 5	1.6 X 1.2	18	50
X 10	0.8 X 0.6	9	25
X 20	0.4 X 0.3	5	13

\*32 x 32 pixel sub-image #pitch of 1/2 subimage

**Table 1 Field of view and resolution of the DIC System**

**Coefficient of Thermal Expansion (CTE) measurement**

The DIC technique is based on thermomechanical deformation measurement and can therefore be used to measure the Coefficient of Thermal Expansion (CTE) of materials. CTE measurements can be used to calibrate DIC.

The calibration principle is to measure the deformation over a known temperature range of a pure material. In this case a 99.9% pure piece of aluminium (source Goodfellow Metals) was used. A 1 cm diameter disc of aluminium was placed on the sample heating chuck and heated from room temperature up to 100 °C. Images of the sample were acquired at 10°C intervals. Image correlation measurements were carried out at each temperature step to yield deformation maps (Figure 7) and a linear plot of thermal expansion versus temperature (Figure 8) was created for the horizontal line through the centre of the metal disc, yielding the CTE.

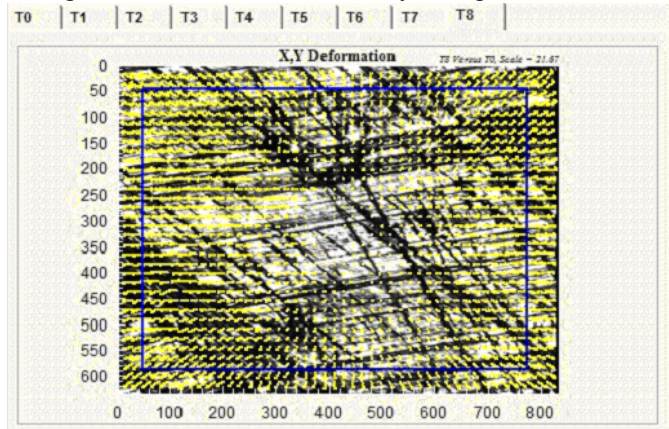


**Figure 7 Deformation map of aluminium showing in blue the area used to measure the CTE.**

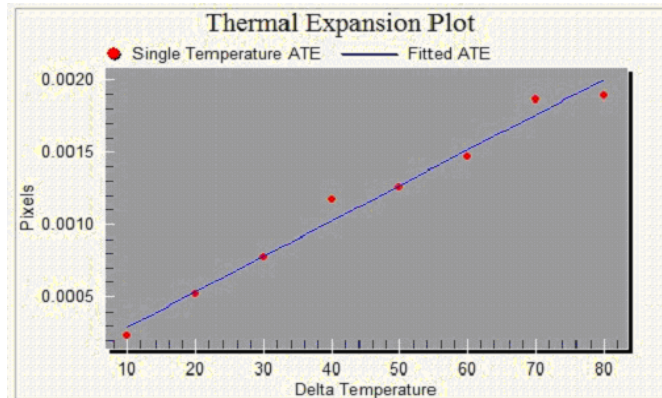


**Figure 8 Thermal expansion linear plot showing the straight line fit from which Apparent CTE is calculated.**

Run number	CTE (ppm)	Fraction from 25.11	$\sigma$ mean	Fraction from book value 24.00	$\sigma$ book
1	25.25	0.10		0.72	
2	26.65	1.15		1.52	
3	26.05	0.70		1.18	
4	26.01	0.67		1.15	
5	24.44	-0.50		0.25	
6	22.17	-2.19		-1.05	
7	24.37	-0.55		0.21	
8	25.94	0.62		1.11	
Mean	25.11				
Standard Deviation ( $\sigma$ )	1.34 (5.34% of mean)				

**Table 2 CTE values obtained from a series of eight repeat measurements on aluminium.** The mean value of CTE obtained lies within one standard deviation ( $\sigma$ ) of the expected value of 24 ppm/°C for Aluminium of 100 % purity. (source: Matweb). Note that the CTE would be expected to increase with temperature.

**Warpage and Rigid Body Rotation Correction**

The effect of warpage is also discussed in this paper, and in particular, its influence on DIC results as an apparent rigid body rotation. This apparent ‘rotation’ is not actually rotation about the bump but is due to the warpage of the sample causing a rotary motion in the field of view about an off-field point. After correction for rigid body translation the warpage appears as rotation. The apparent rotation is explained schematically in Figure 9. When the package warps upward, its effect is to rotate the five sample points marked in black to the positions marked in red.

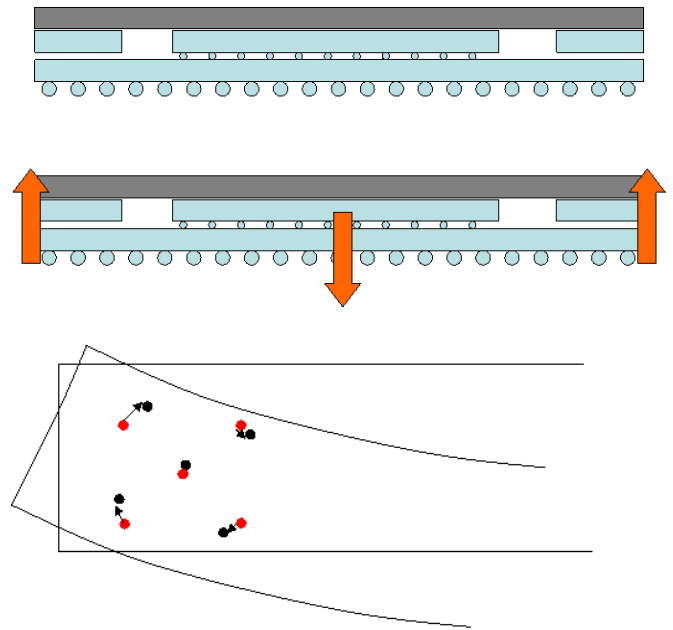


**Figure 9 Warpage effect of FCPGA packages**

## Sample Preparation for Digital Image Correlation

Digital Image Correlation (DIC) relies upon the appearance of “fingerprint” digital greyscale patterns locally over as much of the sample as possible. DIC will therefore perform best on samples, and regions thereof, which have an optically observable microtexture, but which are macroscopically smooth. A simple rule is that the part of the sample to be inspected should not specularly reflect light, but should scatter it. Taking the wavelength of visible light as approximately 0.5 micron, samples having a roughness average of several micron may be expected to produce a highly microtextured image, which will facilitate the measurement of deformation. Such non-specular surfaces are the ideal for image correlation analysis. To obtain the best results with DIC using the X5 or X10 objectives, a sample preparation of successively finer polishing of cross-sectioned samples back to a 1 micron grit is required, followed by a controlled roughening of the cross section surface using typically a 3 micron grit. 1200 grade abrasive paper is typically used for about 30 seconds to produce a suitable microtexture.

### Goodness of data

The technique is equipped with a correlation threshold tool, which allows the correlation parameter (which runs from 0% to 100%) to be set at a minimum acceptance level, typically 99%, and shows the contours in variation of the top two percentiles of correlation parameter. Regions below 99% correlation have their corresponding vectors are screened out of the deformation vector maps. The results presented here used a correlation parameter filter of 99% to filter out poorly correlated data, explaining the occasional local absence of a vector in certain plots. Poor correlation can occur for a variety of reasons, including poor microtexture, local micro-deformation within a material changing its light scattering characteristics, and gross rigid body motion in the case of a sample which shifts significantly during measurement. It is general practice to mechanically constrain samples as little as possible when mounting them.

### Digital Image Correlation of Flip Chip - BGA Packages

Image correlation measurements were made on two FCBGA packages using an OMISTRAIN<sup>®</sup> 1000 Digital Image Correlation strain measurement system using a 10X objective. Each sample was run through a temperature cycle from 20 °C to 100 °C with a 10 minute settling time at 100 °C.

The reference point for motion in each deformation vector map image is calculated globally using approximately the central 2/3 of the image, and plotting the vectors such as to give a zero resultant within this region. In some of the images, a local referential area is set. This is indicated as a blue rectangle on the relevant images, and the resultant is set to zero within this area, which is selected for uniformity of its motion so that it becomes the effective zero referential point of the image.

The scale factor indicated in the top right hand corner of the deformation maps indicates the magnification factor at which the vectors are plotted. The field of view of the sample

under measurement is displayed in microns. The strain in Y, and shear strain maps, are in parts per million.

## Results and Discussion

Both samples were measured at locations at the edge of a row of solder bumps as shown in Figure 10 below.

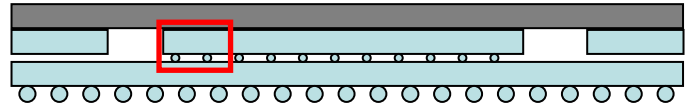


**Figure 10** Diagram showing location of measurement in each FCBGA sample

Figure 11 and 12 shows the reference micrograph fields of view as schematics, with the main features labeled.

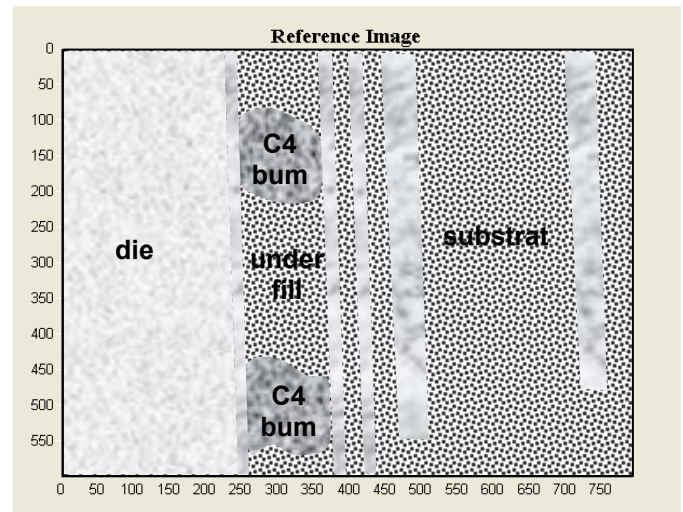


**Figure 11** Schematic of FCBGA sample A.

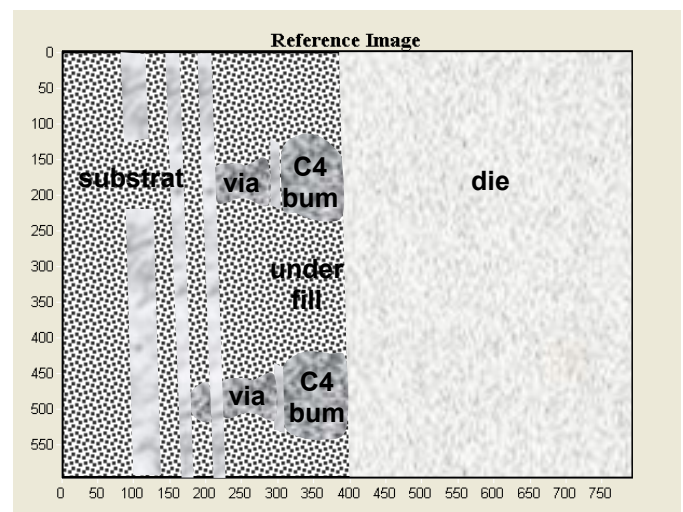


**Figure 12** Schematic of FCBGA sample B

Figures 13 to 24 show the results obtained on both FCBGA samples using Digital Image Correlation. Deformation maps at 50°C and 100°C are shown, before and after rotation correction. Shear and Strain in X maps are also presented for the 100°C case.

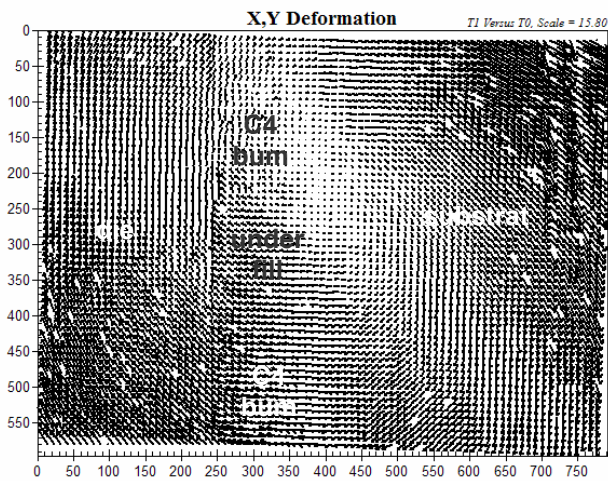


Figure 13 Deformation map for sample A at 50°C, before rotation correction. Vectors magnified by 15.80.

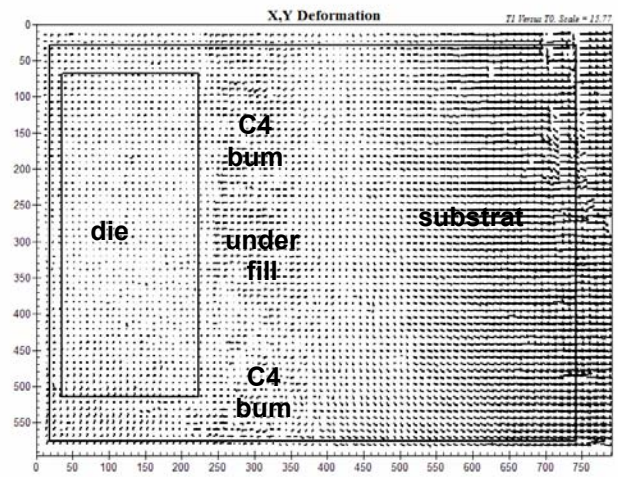


Figure 16 Deformation map for sample A at 50°C, after rotation correction within large box, and local reference zero within small box. Vectors magnified by 15.77.

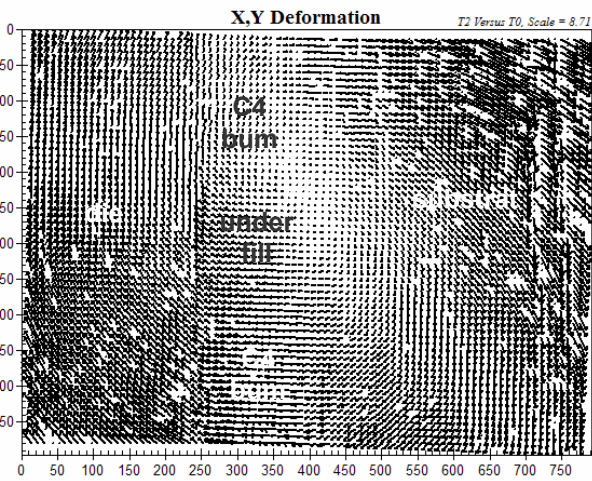


Figure 14 Deformation map for sample A at 100°C, before rotation correction. Vectors magnified by 8.72.

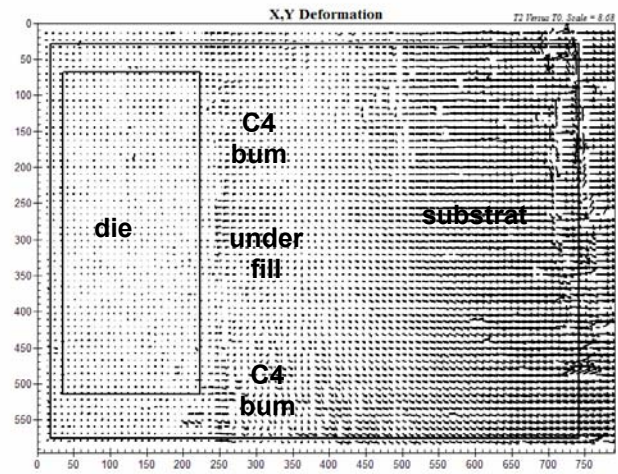


Figure 17 Deformation map for sample A at 100°C, after rotation correction within large box, and local reference zero within small box. Vectors magnified by 8.68.

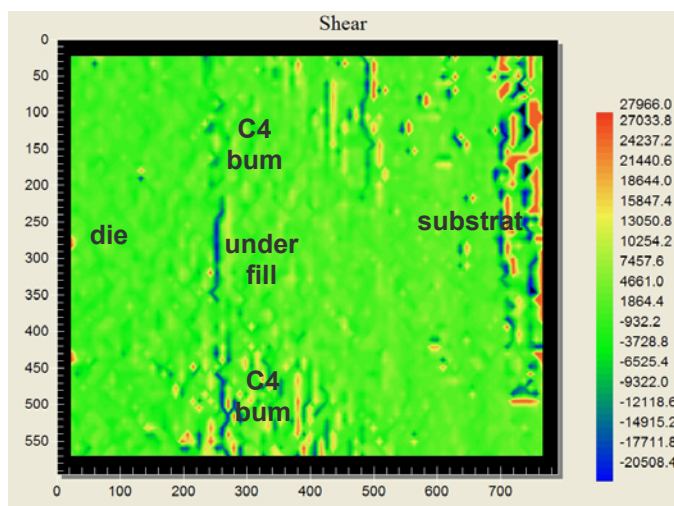


Figure 15 Shear map for sample A at 100°C

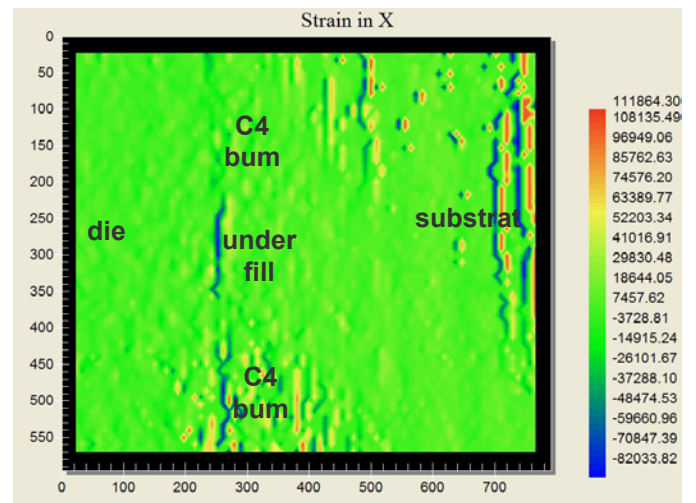


Figure 18 Strain in X map for sample A at 100°C

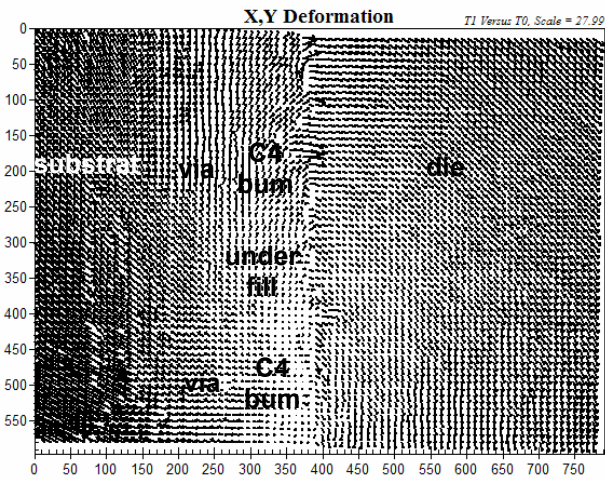


Figure 19 Deformation map for sample B at 50°C, before rotation correction. Vectors magnified by 27.99.

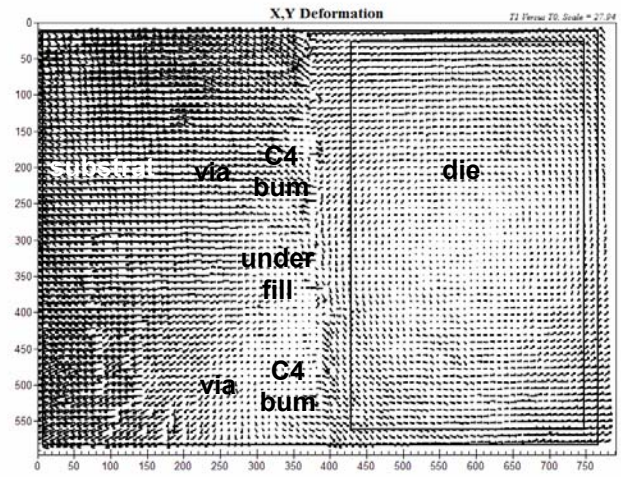


Figure 22 Deformation map for sample B at 50°C, after rotation correction within large box, and local reference zero within small box. Vectors magnified by 27.94.

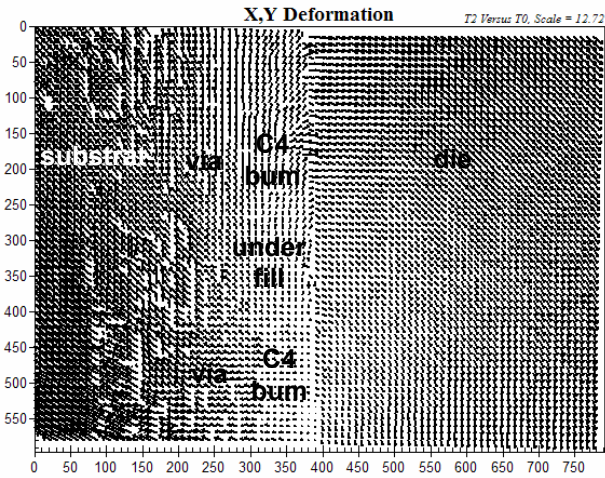


Figure 20 Deformation map for sample B at 100°C, before rotation correction. Vectors magnified by 12.72.

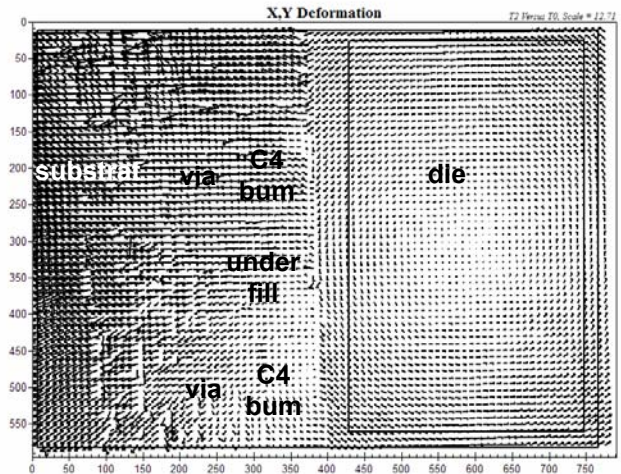


Figure 23 Deformation map for sample B at 100°C, after rotation correction within large box, and local reference zero within small box. Vectors magnified by 12.71.

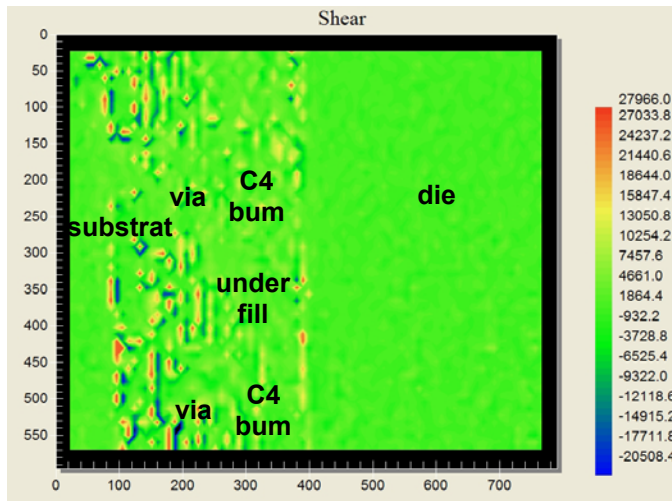


Figure 21 Shear map for sample B at 100°C

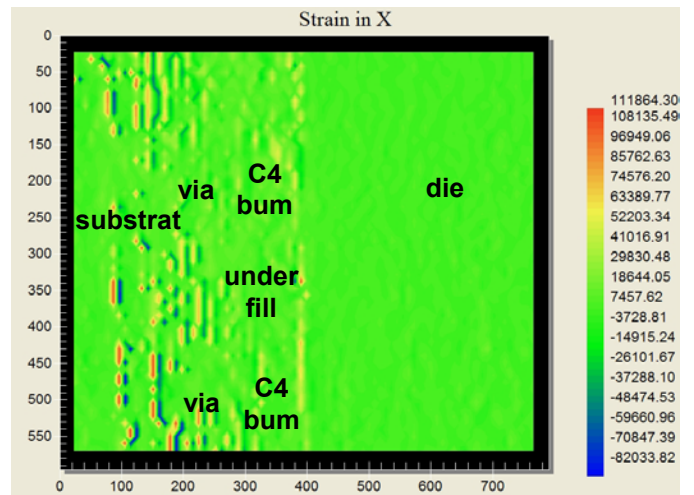


Figure 24 Strain in X map for sample B at 100°C

Figures 13 and 14, and Figures 19 and 20 show the corresponding deformation maps acquired for samples A and B, at temperatures of 50°C and 100°C, respectively. Because of the effect of warpage the deformation map includes a sizeable rigid body rotation effect. In order to determine accurately the deformation map without the influence of the rigid body effect a rotation correction algorithm was developed in order to subtract this underlying effect. Figures 16 and 17, and Figures 22 and 23 show the corresponding deformation maps acquired for samples A and B, at temperatures of 50°C and 100°C, respectively, with the rotation removed.

This rigid body rotation correction has no significant effect on the derivative maps to calculate strain and shear, since the correction variation is gradual across the entire field of view, rather than a sharp localised change. Strain and shear maps are therefore calculated without rigid body rotation correction.

When the rigid body rotation is removed, the sharp difference in the motion characteristics of the die, the C4 layer, and the substrate are highlighted.

In order to further highlight these locations on each sample where there exists a high, localised strain, shear maps and strain in X maps were calculated as derivatives of the deformation maps. Figures 15 and 21 show the shear maps calculated for samples A and B, respectively. Figures 18 and 24 show the shear maps calculated for samples A and B, respectively. These results show clearly a high concentration of thermomechanical shear strain at the interface region of the silicon die and the flip chip bumps, in the flipchip/underfill layer itself, and also at interface regions in the substrate. These are the most critical locations in the FCBGA package.

In sample A, we observe a strongly compressive strain between parts of the C4 layer and the substrate, with relatively little comparable strain in the substrate. By contrast, we see that in the sample B, that the most pronounced local strain is actually in the substrate material itself, rather than in the C4 layers. In this case, the substrate region examined had a greater visible metallic layer content, and also had via contacts to the C4 bumps. Substrate materials and their structure play a critical part in determining the overall strain characteristics of the package.

Motion analyses of this type take relatively little time to perform using digital image correlation, and the measurement cycle used in this paper takes approximately one hour to run on the equipment used, generating a full results set. It can nevertheless provide a powerful insight into the complex thermo-mechanical behaviour of the package, even at moderate temperature excursions, as evidenced by the emergence of characteristic motion patterns on heating from 20°C to 50°C.

## Conclusions

It has been shown that digital image correlation is an extremely useful technique for the characterization of thermomechanically induced strain in microelectronic packages, in particular Flip Chip on BGA packages which present with some unique strain problems. The usefulness of DIC has been shown to be enhanced by an accurate

calibration of the technique using materials of known thermomechanical properties. It has also been shown that measurements may be effected by the effect of warpage. This is very noticeable in the case of FCBGA packages. This warpage leads to rigid body rotation which must be subtracted from the measurements in order to extract accurate deformation maps. The technique is particularly suited to detecting locations where higher strain concentrations may lead to future failures. In the case of FCBGA this ability may be used in determining the potential for failure at the die/bump interface which is the critical zone for strain analysis in the package, as well as revealing the complex strains within substrates.

## References

- 1 Pitter M.C., See C.W., Somekh M.G., Subpixel microscopic deformation analysis using correlation and artificial neural networks, *Optics Express*, Vol 8, No. 6, pp 322-327, 2001
- 2 Pendse R.D., Zhou P, Methodology for Predicting Solder Joint Reliability in Semiconductor Packages, *Microelectronics Reliability* 42, pp 301-305, 2002
- 3 B. Han, "Recent Advances of moiré and microscopic moiré interferometry for thermal deformation analyses of microelectronic devices", *Experimental Mechanics*, Vol. 38, pp 278-288, 1988
- 4 Han B, Guo Y, Lim CK, Caletka D., Verification of numerical models used in microelectronic packaging design by interferometric displacement measurement methods, *ASME J Electronic Packaging*, 118, pp 157-163, 1996